Warm and saline events embedded in the meridional circulation of the northern North Atlantic

Sirpa Häkkinen,[1] Peter B. Rhines,[2] and Denise L. Worthen[3]

Received 16 March 2010; revised 1 November 2010; accepted 21 December 2010; published 4 March 2011.

[1] Ocean state estimates from 1958 to 2005 from the Simple Ocean Assimilation System (SODA) system are analyzed to understand circulation between subtropical and subpolar Atlantic and their connection with atmospheric forcing. This analysis shows three periods (1960s, around 1980, and 2000s) with enhanced warm, saline waters reaching high latitudes, alternating with freshwater events originating at high latitudes. It complements surface drifter and altimetry data showing the subtropical-subpolar exchange leading to a significant temperature and salinity increase in the northeast Atlantic after 2001. The warm water limb of the Atlantic meridional overturning cell represented by SODA expanded in density/salinity space during these warm events. Tracer simulations using SODA velocities also show decadal variation of the Gulf Stream waters reaching the subpolar gyre and Nordic seas. The negative phase of the North Atlantic Oscillation index, usually invoked in such variability, fails to predict the warming and salinization in the early 2000s, with salinities not seen since the 1960s. Wind stress curl variability provided a linkage to this subtropical/subpolar gyre exchange as illustrated using an idealized two-layer circulation model. The ocean response to the modulation of the climatological wind stress curl pattern was found to be such that the northward penetration of subtropical tracers is enhanced when amplitude of the wind stress curl is weaker than normal. In this case both the subtropical and subpolar gyres weaken and the subpolar density surfaces relax; hence, the polar front moves westward, opening an enhanced northward access of the subtropical waters in the eastern boundary current.

Citation: Häkkinen, S., P. B. Rhines, and D. L. Worthen (2011), Warm and saline events embedded in the meridional circulation of the northern North Atlantic, *J. Geophys. Res.*, *116*, C03006, doi:10.1029/2010JC006275.

1. Introduction

[2] The waters originating from the western boundary current form the North Atlantic Current (NAC), with some of its branches diverted toward the Nordic seas (Figure 1). These northward flowing branches of NAC show distinct low-frequency variability with alternating periods of warm and salty waters and cool and freshwaters in the multidecadal hydrographic records from the NE North Atlantic Ocean, from Rockall Trough and Faroe Shetland Channel [*Reverdin et al.*, 1997; *Belkin et al.*, 1998; *Holliday et al.*, 2008]. The fresh events appearing in the northeastern Atlantic are advected from the western subpolar region by the cyclonic gyre circulation [*Dickson et al.*, 1988; *Belkin et al.*, 1998; *Reverdin et al.*, 1997]. These fresh salinity anomalies are dissipated very slowly and can be identified 10 years or later in the northern reaches of the Nordic seas. One such low-salinity event in the eastern subpolar gyre followed the intensely windy early 1990s, followed by a recovery to salinity values of the mid-1980s [*Holliday et al.*, 2008]. This salinization and warming of the subpolar gyre continued further after 2001 (at least to 2009) with salinity values not seen since the 1960s [*Reverdin*, 2010]. The surge of warm and saline water reaching the eastern subpolar gyre and northward to the Norwegian Sea and Barents Sea is especially well documented [e.g., *Hansen et al.*, 2008, *Holliday et al.*, 2008, *Sarafanov et al.*, 2008]. The decadal variation of this northward penetration of warm waters plays a role in global warming analysis, since the Atlantic sector contributes substantially to the hemispheric mean surface temperature empirical orthogonal functions (EOFs) (J. M. Wallace and B. V. Smoliak, private communication, 2010). The longer timescale Atlantic Multidecadal Oscillation (AMO) [e.g., *Enfield et al.*, 2001] may also project onto the intergyre communication addressed here.

[3] We examine the advective pathway from the subtropics to subpolar gyre, but it is likely that the warm, saline periods can have multiple causes. The recent warming occurred nearly simultaneously over much of the ocean between Rockall (57°N) north to the Fram Strait (78°N) (*Holliday et al.* [2008] suggest a 3–4 year time lag to reach the northernmost latitudes.) This widespread coordination implicates

[1]NASA Goddard Space Flight Center, Greenbelt, Maryland, USA.
[2]School of Oceanography, University of Washington, Seattle, Washington, USA.
[3]Wyle ITS and NASA Goddard Space Flight Center, Greenbelt, Maryland, USA.

Copyright 2011 by the American Geophysical Union.
0148-0227/11/2010JC006275

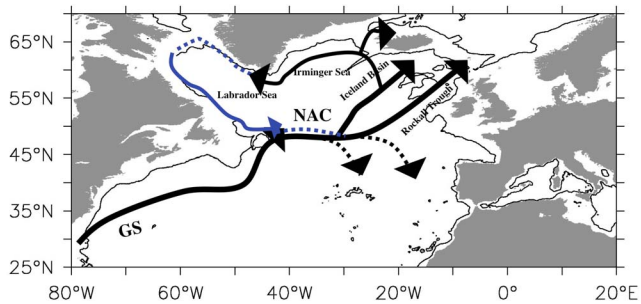

Figure 1. Map of the North Atlantic Ocean and its major currents, the Gulf Stream (GS) and North Atlantic Current (NAC) branches.

air/sea heat flux in the variability. However, the warm subtropical waters extend far beneath the ocean surface (typically to 1000 m), and their decadal variability does as well. In addition, at least in Rockall Trough in the late 1990s, *Holliday* [2003] shows variations in the column storage of heat and freshwater to exceed greatly the change in air/sea heat and freshwater fluxes. Regarding the saline water inflow in general, two sources have been proposed: the North Atlantic Current (NAC) modified by mixing with Mediterranean Waters [*McCartney and Mauritzen*, 2001] and Eastern Atlantic Waters [*Pollard et al.*, 2004]. An extensive analysis of climatological mean pathways of the northward moving warm waters by *Brambilla and Talley* [2008] and *Brambilla et al.* [2008] describes their multiple paths, relationship with the subpolar gyre circulation, and connection with mode water formation and water mass transformation and particularly emphasizes the role of air/sea buoyancy fluxes. The potential vorticity minima associated with subpolar mode waters originate in deep wintertime mixing and imply a consistent pattern of subduction and obduction of eastern subpolar surface waters.

[4] *Hakkinen and Rhines* [2009] (hereafter referred to as HR2009) show that Gulf Stream waters, as indicated by surface drifters, can, in fact, have a direct connection to the Rockall region as a likely explanation for the significantly higher inflow salinities since 2001. The change in the surface circulation, which redirects part of the saline waters to NE instead of SE with the gyre circulation, would not need mixing with the Mediterranean waters to increase the inflow salinity. However, there is evidence that the Mediterranean waters also penetrated more northward during these salty periods [*Lozier and Stewart*, 2008; *Johnson and Gruber*, 2007].

[5] Our main objective is to investigate whether the direct connection between the Gulf Stream waters and NE North Atlantic occurred in the earlier times. Since these northward flowing Gulf Stream/NAC waters form the upper limb of the Atlantic meridional overturning cell (AMOC), we will explore how changes in the pathways are reflected in the structure of the AMOC. Our second objective is to investigate linkages between the pathway changes and the atmospheric circulation patterns. We note that *Reverdin et al.* [1997] did an excellent analysis on the relationship of the atmospheric forcing and the subpolar upper ocean salinity content and found the positive salt content to be linked with negative North Atlantic Oscillation (NAO). With a longer record available we revisit the atmospheric analysis with a focus on the wind stress curl. Finally we present simulations using an idealized isopycnal two-layer model when forced with simple wind stress curl variability to describe spreading of tracers from the subtropics.

2. Data

[6] We concentrate on data from Simple Ocean Assimilation System (SODA) by *Carton et al.* [2000] and *Carton and Giese* [2008]. It spans years 1958 through 2007 and is available with monthly time resolution. The data set we are using is retrieved from the IRI/Lamont-Doherty Ocean Data Depository (http://iridl.ldeo.columbia.edu). IRI data set is a regridded SODA output interpolated into a uniform horizontal resolution of 0.5°, with 46 vertical levels with thickness ranging from 5 to 300 m. The SODA data set is forced using ECMWF winds (ERA-40) from 1958 to 2001 after which the wind forcing is constructed from scatterometer (QuikSCAT) derived data set. The available hydrographic data have been assimilated to the model; however, this version does not assimilate the altimeter data from TOPEX/Poseidon or Jason-1.

[7] To compare model results, we use surface currents from NOAA/AOML Global Lagrangian Drifting Buoy Data Base (1989 onward). These drifters are drogued to 15 m depth below sea surface, and their location is reported every 6 h. The lifetime of the drogues varies considerably, but the average life span of the drifters (~271 days [*Brambilla and Talley*, 2006]) has not changed significantly over the years.

[8] The surface wind product used to compute the wind stress curl in our analysis has been replaced by the NCEP/NCAR Reanalysis [*Kalnay et al.*, 1996] wind stresses because the stress product used in SODA and particularly the derived curl has a strong trend (stronger than in NCEP/NCAR product). In fact, removal of a linear trend results in very similar behavior of the first two empirical orthogonal function (EOF) modes as in the NCEP/NCAR derived product. It is not clear if the trend is a bias from moving away from ERA-40 to QuikSCAT. However, the impact of the spurious trend in the model surface forcing is diminished through the assimilation process itself.

3. Results

3.1. Salinity Distribution

[9] The salinity time series at 112 m from SODA across the latitude 60°N is displayed in Figure 2a for longitudes 45°W–2°W. The two main NAC pathways to the Nordic seas, at 14°W and 3°W–8°W, are distinguishable by their local salinity maximum along this latitude. The Faroe Shetland Current has two branches, the "open water" branch at 8°W and the continental slope branch at 3°W [*Hansen et al.*, 2008]. Figure 2a shows two main epochs with highly saline conditions: in the beginning, before 1971, and at the end of the record, after 2003, both with a large westward extent. High salinity values were also present 1980–1985 but the values above 35.28 psu have a limited westward extent compared to the two main periods. Figure 2a also shows the arrival of the fresh events of the 1960s in 1975, 1980s, and weaker events of the 1990s in the eastern basin. SODA data gives the long-term average salinity at 15 m at 60°N in the Iceland Channel

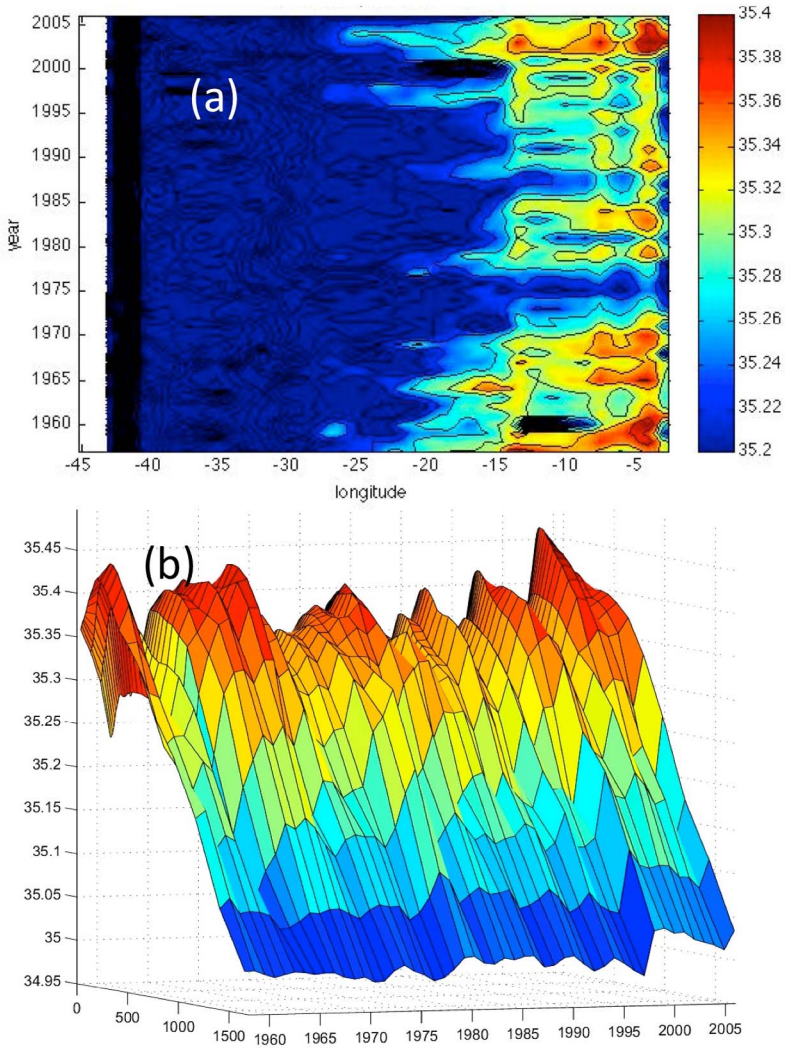

Figure 2. (a) SODA salinity distribution at 112 m across 60°N. (b) Annual salinity distribution averaged from 32.75°W to 9.75°W at 55°N in time-depth space defined by SODA vertical layers down to 1625 m.

and Rockall Trough to be 35.246 psu and 35.249 psu, respectively.

[10] Another view to the salinity variability is given at 55°N averaged over longitudes 35.75°W to 9.75°W which is displayed in a three dimensional space of time and vertical depth layers down to 1625 m in Figure 2b. Figure 2b shows that the saline events are surface intensified and extend down to 1000 m, below the depth of wintertime convection.

3.2. Surface Circulation and Advection of Tracers

[11] In the warm subtropical Atlantic surface waters temperature and salinity are positively correlated, but the salinity has a weaker impact on density variations, and hence, it acts as a tracer for subtropical waters. This motivates our tracer advection experiments using SODA velocity fields to investigate the salinity variability in the NE Atlantic. For comparison, we also apply the surface velocity field constructed from independent surface mixed layer drifter observations described in HR2009. To improve the representativeness of the drifter velocity field, the drifter velocities are binned into 1° × 1° boxes by creating 5 year averages starting in 1991. This approach using constant pentadal velocity is adopted also for the SODA data starting from 1961. The compilation into pentads captures the major epochs of low and high NAO years, such as 1966–1970 containing the most negative NAO index years of the 20th century, and the 5 year averages correspond also to typical adjustment times for the subtropical gyre.

[12] Our tracer model simply solves the advection equation $\partial S/\partial t = -\mathbf{v} \cdot \nabla \mathbf{S}$. This is a nonconservative form as we allow the tracer to be lost to the deeper layer in the presence of horizontal convergence. We use forward time differencing for advection and apply *Lin et al.*'s [1994] parabolic scheme to reduce numerical diffusion. The temporally constant tracer field is inserted uniformly to an area over the Gulf Stream, 70°W–48°W, 35°N–42°N, during each 5 year simulation. The tracers will spread away from this box following the constant 5 year average SODA velocity field at 15 m. This simulation is done for each pentad (starting 1961) with the corresponding pentadal velocity field. The

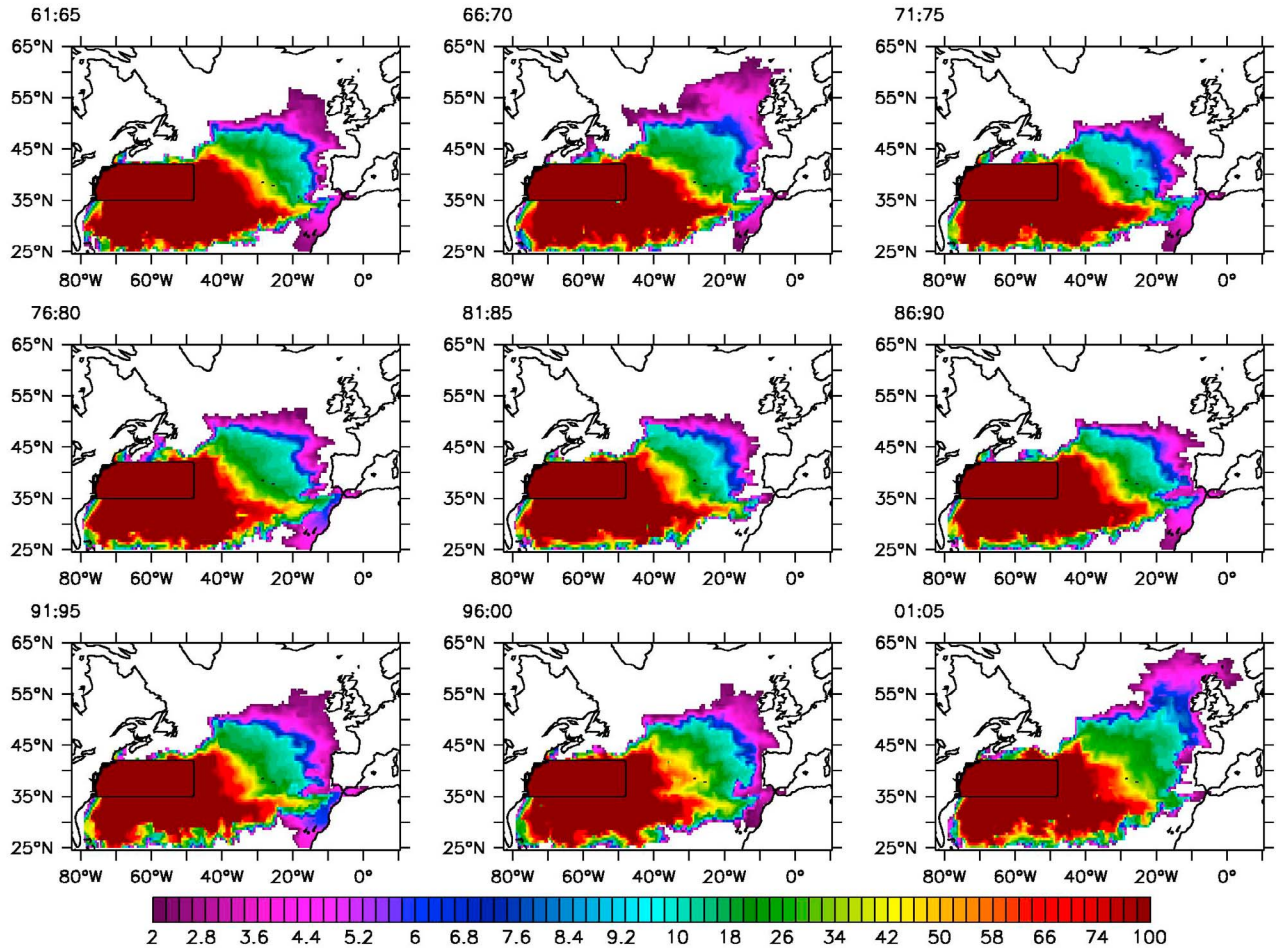

Figure 3. Tracer advection for the 9 pentads (starting 1961) at the end of the 5 year simulation using the SODA 5 year average velocity at 15 m, with tracer values kept constant in the Gulf Stream box.

tracer model has open boundaries at 25°N and 65°N where the tracer is allowed to exit. The experiment using the drifter velocity field followed the same protocol.

[13] The tracer modeling results for each pentad are shown at the end of each 5 year simulation. The near-surface tracer advection from the SODA data is depicted in Figure 3 for nine pentads starting 1961. There are only two pentads, 1966–1970, and 2001–2005 with a prominent advection/diffusion of tracers toward NE and tracers present in the Rockall Trough, but a strong tendency of tracer advection toward NE is already seen in the immediately preceding period. The tracer advection in the entirely independent set of pentad

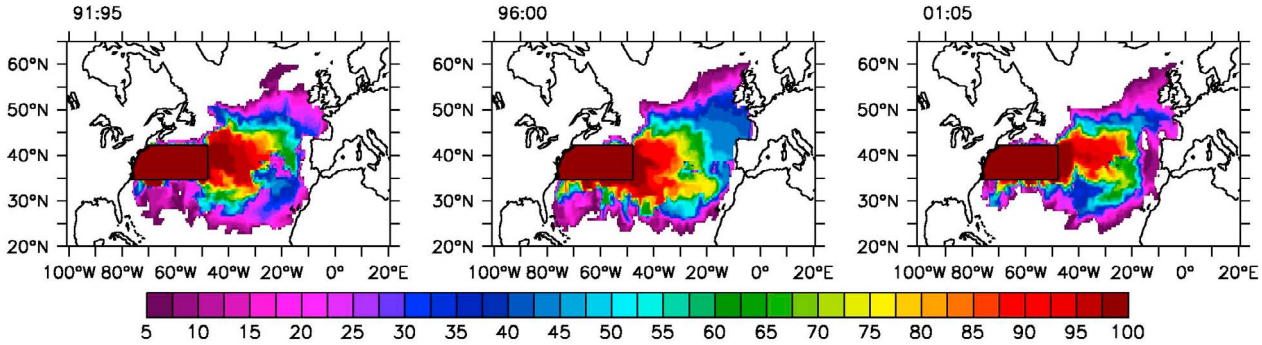

Figure 4. Tracer advection for the final 3 pentads at the end of the 5 year simulation using the 5 year average velocity based on observed surface drifter data (at 15 m), with tracer values kept constant in the Gulf Stream box.

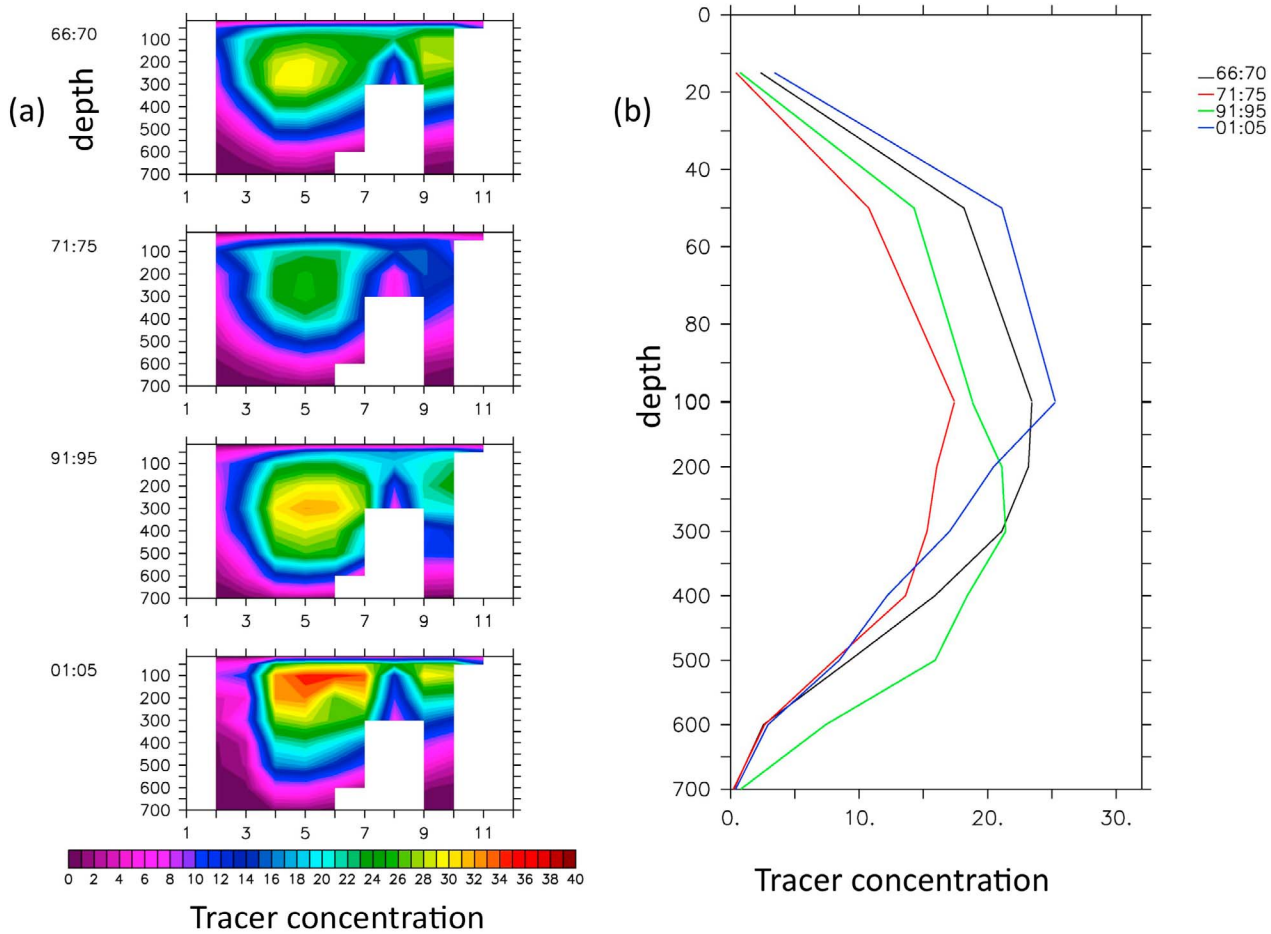

Figure 5. Vertical distribution of tracers for the 4 pentads (1966–1970, 1971–1975, 1991–1995, 2001–2005) at the end of the 5 year simulation using the SODA pentad average velocities for depth range 0–700 m. (a) Vertical distribution in the section crossing from the Iceland Basin to Rockall Trough (20°W, 65°N) (left) to (10°W, 55°N) (right). (b) Sum of the tracer concentration in the same section versus depth. Tracer values kept constant in the Gulf Stream box.

average drifter velocity fields (from drifter observations) starting 1991 is shown in Figure 4. Behavior is very similar as found in the SODA near-surface advection, but the 1996–2000 period shows as a high tracer concentration as the last period, 2001–2005. In the drifter observations, the last two periods have 15% of the original tracer value present west of the British Isles compared to about 5% using SODA data. This difference may simply be an ocean model bias toward weaker NAC and exchange with the Nordic seas. The more important aspect is the success of the SODA assimilation recreating the surface circulation changes to connect Gulf Stream waters with the NE corner in the 1960s and since 1996 and to produce the lack of intrusion of high-salinity surface waters northeastward between 1971 and 1995. The use of 5 year mean velocity fields omits eddy variability yet seems to capture the observed northward invasion of warm and salty waters.

[14] The SODA data can also shed light on the subsurface advection field. Using pentad average velocities at deeper levels, the tracer advection was computed with a constant source at depth (at SODA z levels down to 700 m) as in Figure 3 experiment. We chose pentads 1966–1970, 1971–1975, 1991–1995, and 2001–2005 as representative of the saline and fresh years in the NE Atlantic. Figure 5a shows a tracer distribution for these pentads in a section from (10°W, 55°N) to (20°W, 65°N), encompassing Rockall Trough and the Iceland Basin. Except for the last pentad, tracer concentration forms a subsurface peak at 200–300 m in the Iceland Basin, while the peak in Rockall Trough lies at 50–250 m. The last pentad 2001–2005 shows the maximum concentration with almost 20% higher values at around 100 m in both channels. Figure 5b shows the integrated tracer concentration in the same section. The largest changes in the tracer concentration occur in the top 100 m between the fresh and the saline pentads, of the order of 20%–30% at 100 m. The observed salinity history (Figure 2) shows that the advective changes reach deeper than 700 m in the water column, and independent study using the FLAME 1/10° resolution model (K. Burkholder, private communication, 2010) suggests that the maximum intergyre exchange occurs several hundred meters below the surface.

[15] The SODA near-surface field was also used in a set of 5 year simulations where the Gulf Stream box was initialized with a constant tracer field but then allowed to

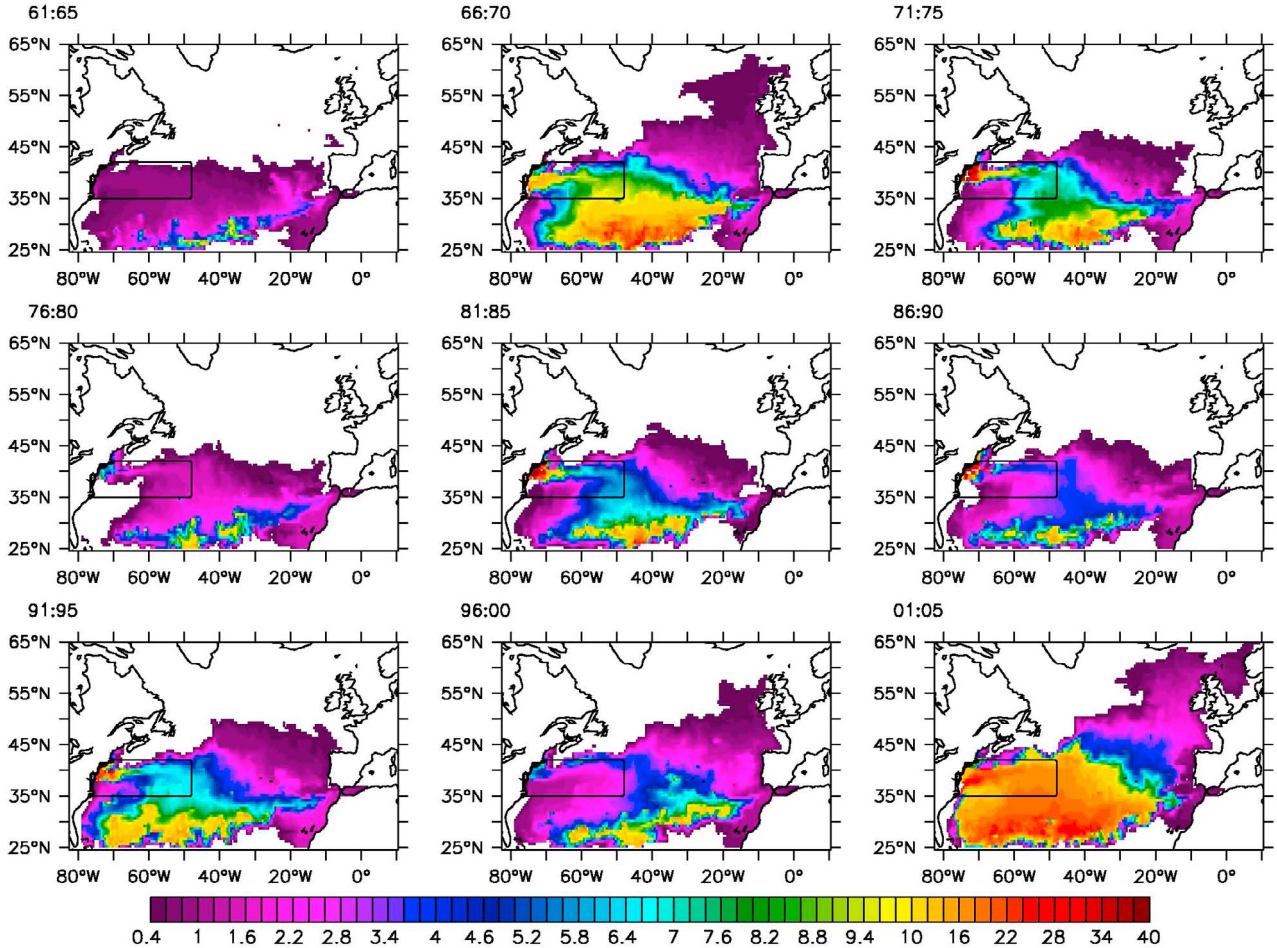

Figure 6. Tracer advection for the 9 pentads at the end of the 5 year simulation using the SODA 5 year average velocity at 15 m, without updating the tracer concentration in the Gulf Stream box.

evolve freely. The results at the end of each 5 year simulation are shown in Figure 6. While the northward extension of the tracers clearly separates the years in the late 1960s and since 2001 into their own category, the average concentration left in the basin is also very different in these two periods. Since the subtropics is a region of downward Ekman pumping, the flow field is highly convergent, and more tracers should be lost to the deeper layers when Ekman pumping is strong than in the case with a weak Ekman pumping. Since Ekman pumping and the strength of the wind stress curl are associated, the surface circulation in the subtropical gyre must also be weaker in these two periods compared to the other seven pentads. This is discussed further in section 4.1 in connection of the wind stress curl variability, with a further corroboration from the idealized two-layer model experiments in section 4.2.

3.3. AMOC

[16] Northward penetration of warm subtropical waters is an essential branch of the AMOC. While the deep southward branch and its boundary currents would seem to be remote from these events, there is evidence that through entrainment in the sinking, dense overflows, upper ocean trends are rapidly communicated to the deep water [*Yashayaev et al.*, 2007]. Year-by-year evolution of the Iceland-Scotland Overflow Water in the Iceland Basin shows evidence of both the fresher, cooler early 1990s and the warmer, more saline 2000s. The MOC image of the events described here is clear in the SODA assimilation. Plotted against potential density, the upper AMOC at high latitude is dominated by the eastern subpolar gyre owing to the sloping isopycnal topography.

[17] The time mean AMOC in the latitude-density space for SODA data is shown in Figure 7. It has two local enhancements centered around 55°N and 35°N–40°N. Also a counterclockwise (mainly freshwater) cell with a strength of 3–5 Sv in the lighter densities is visible north of 45°N. The maximum AMOC at 55°N centered at the densities 27.7–27.8 has fluctuated between 12 and 25 Sv (not shown), rather too large an amplitude to be realistic. These fluctuations occur independently of the freshwater cell variability which was relatively weak in the 1960s, during 1974–1980, and after 1995, and the intervening years were years of spreading of the great salinity anomaly years in the subpolar gyre [*Belkin et al.*, 1998], now identifiable in the AMOC.

[18] The pentads in the early 1990s and early 2000s are quite different based on the tracer advection experiments and surface drifter tracking (HR2009) hence they can provide an example of the change in AMOC in density space. The change

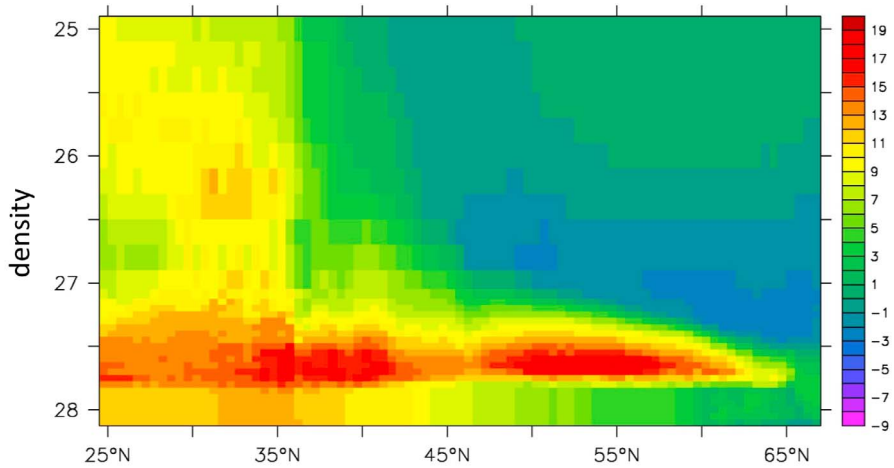

Figure 7. Average AMOC (in Sv) in density space for SODA. Positive values correspond to clockwise circulation in the density-latitude plane.

[2001–2005] minus [1991–1995] is shown in Figure 8. North of 50°N the deep AMOC cell has weakened but the lighter water near the surface (upper thermocline cell) has increased as one would expect from the tracer experiments. At lower latitudes the differences are not uniform, but there is a tendency toward increased AMOC around the thermocline waters (27.3–27.8). Densities less than 27.0 display a weakening cell, interrupted by a strengthened cell centered at densities 26–27.3 at the Gulf Stream extension/southern latitudes of NAC (38–42°N). The strengthening cell at densities 26–27.5 at 38–40°N could be interpreted as the northward displacement of the subtropical gyre.

[19] The strengthened cell north of 50°N in the above thermocline waters represents the difference in the northward subtropical water transport between the period 2001–2005 and 1991–1995 as depicted by the tracer experiments. To support this association, we show the net northward transports at 55°N for salinities over 35.3, 35.4 and 35.5 psu in Figure 9. The time series (Figure 9) show significant net northward transport changes of high-salinity components before 1970, 1978–1983 and after 1999 with factor of 2–3 increase for salinities above 35.3 and above 35.4, and an order of magnitude increase for the waters above 35.5 compared to the intervening years. The transport changes reflect the change in the composition of the AMOC upper limb, while SODA model is inconclusive on changes in AMOC strength at those times. We acknowledge that there may be bias in estimating the transports using the monthly data, however, using annual data gives very similar fluctuations of the transports. Combined with the tracer experiments we have shown that changes in the surface circulation can have a large effect on the salt transport to the higher latitudes. In fact, it appears that change in the circulation is necessary to create these salinity anomalies in the northeast Atlantic.

4. Wind Stress Curl and NAO

4.1. Wind Stress Curl EOF Modes and Saline Water Advection

[20] The negative NAO phase has been already indentified as a predictor of the high-salinity events in the subpolar gyre, but the salinization after 2001 does not appear to fit the pattern.

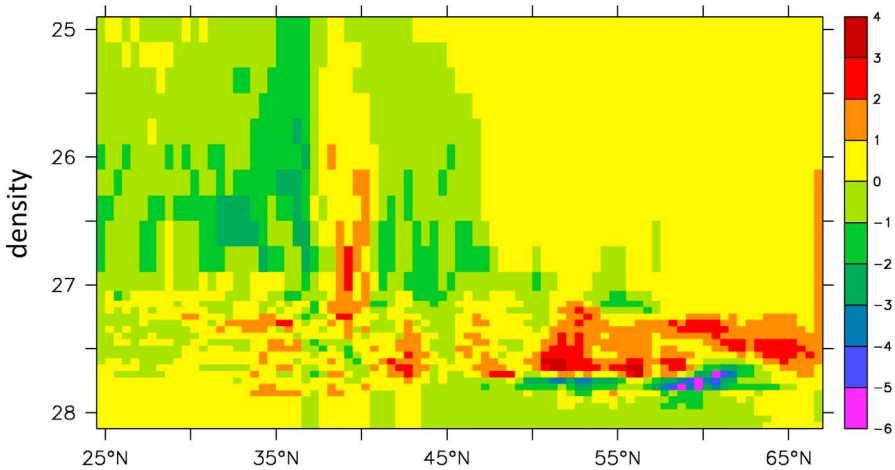

Figure 8. AMOC (in Sv) difference [2001–2005] minus [1991–1995], from SODA. Positive values correspond to clockwise circulation anomaly in the density-latitude plane.

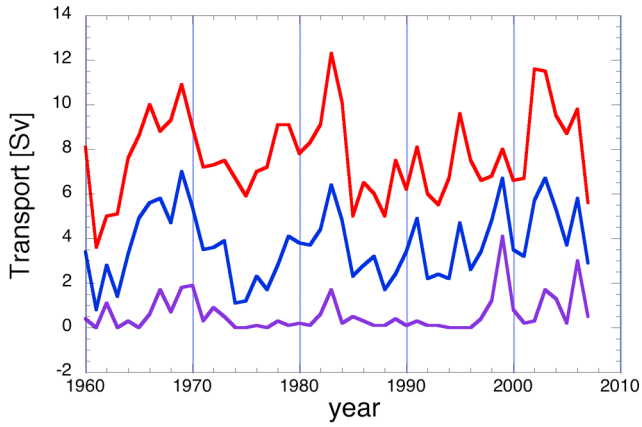

Figure 9. Transport (in Sv) of waters with salinities over 35.3 (red), 35.4 (blue) and 35.5 (purple) psu at 55°N in SODA.

We focus on the wind stress curl because of its direct linkage to gyre strength and circulation. Figure 10 shows the evolution of pentadal wind stress curl of the winter months December–March. The late 1960s and the late 1970s show similar pattern as the early 2000s which we had identified as a potential forcing mechanism in HR2009; hence, the wind stress curl forcing is consistent for the subpolar high-salinity periods. We perform an empirical orthogonal function (EOF) analysis of the wind stress curl for which we use only December to March averages. The spatial patterns of the first two wind stress curl modes are shown in Figures 11a and 11b and the low-pass-filtered principal components (PCs) in Figure 11c. The EOF1 with 26% of the variance has the most prominent center of activity on the subtropical and subpolar gyre boundary at about 50°N. The NAO index projects most strongly on the time series of this mode (correlation 0.78), because the center west of the British Isles is very pronounced with a strongly positive NAO (as can be seen for the pentads 1971–1975 and 1991–1995 in Figure 10). This mode is found to influence the Gulf Stream location [e.g., *Rossby et al.*, 2005]. On the other hand, the EOF2 with 17% of the variance has centers of activity located at the North Atlantic climatological sea level pressure centers of activity (in the Iceland Sea and at Azores), so it represents the modulation of the climatological pattern of the wind stress curl, which is the fundamental forcing of the subpolar-subtropical gyre system. The EOF2 time series has a correlation of only 0.47 with NAO index (albeit significant at 95% level). These EOF patterns relate also to the variability in

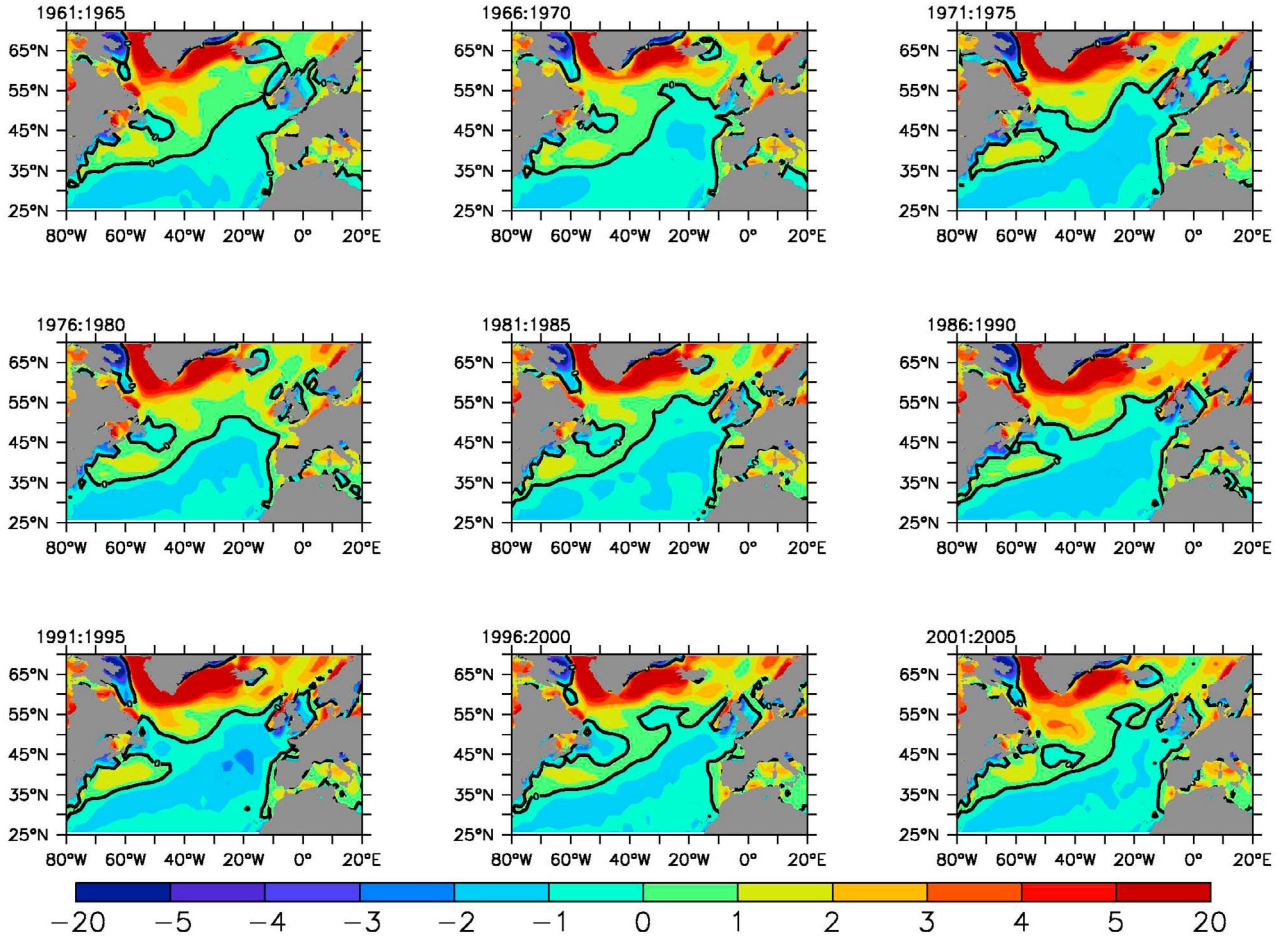

Figure 10. Winter (DJFM) wind stress (from NCEP/NCAR Reanalysis) for pentads starting 1961 in units of 10^{-7} N m^{-3}.

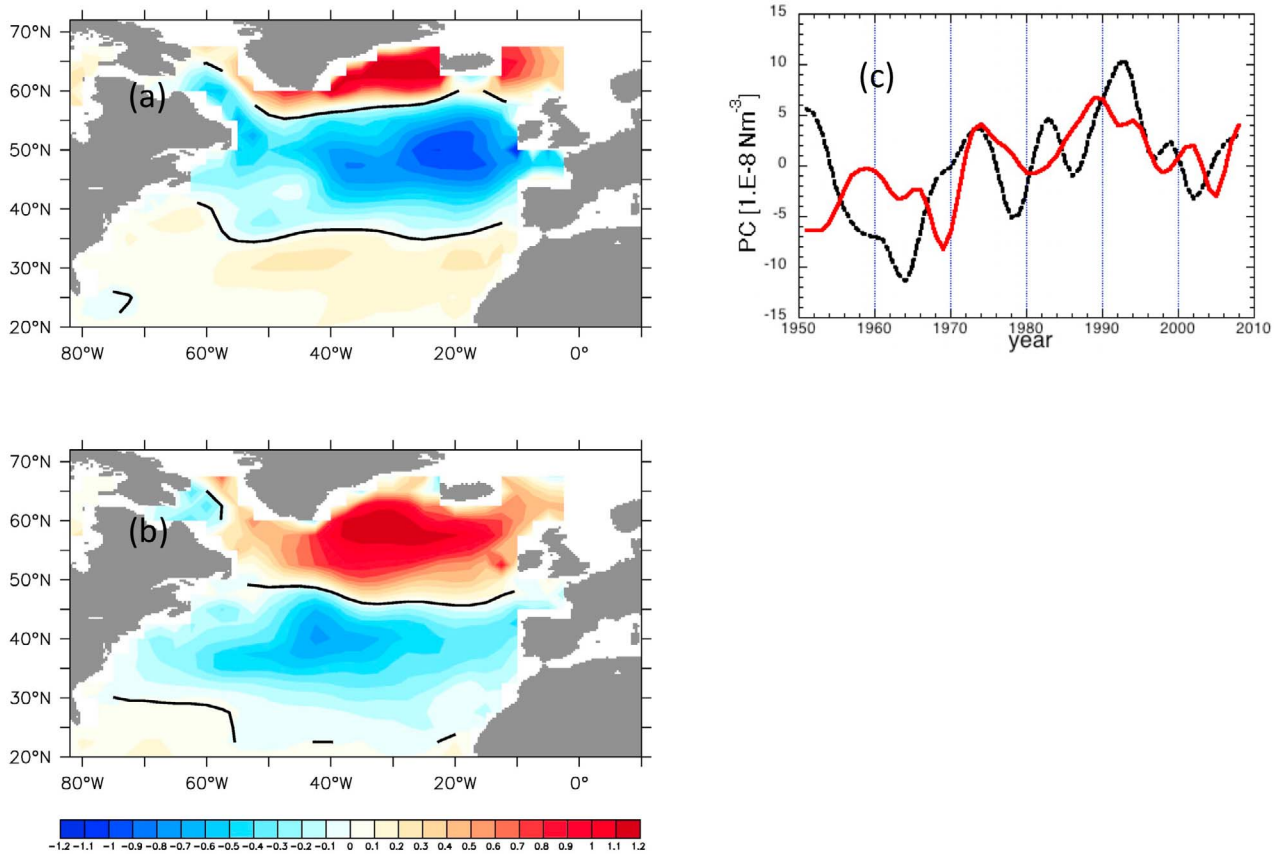

Figure 11. (a and b) Wind stress curl (from NCEP/NCAR Reanalysis) EOFs (26% and 17%; unitless) and (c) the smoothed PC1 (black) and PC2 (red).

the Atlantic storm track over similar timescales [e.g., *Harnik and Chang*, 2003].

[21] Another interesting linkage to the curl EOF2 arises with the transport of the highest salinity waters at 55°N, the transport maxima in broad terms coincide with the local minima of the curl PC2 (i.e., a weak anticyclonic stress over the subtropics). This coincidence is highlighted further in Figure 12 for low-pass-filtered (suppressing periods of less than 5 years) time series and removing a quadratic trend in the PC2 (clearly the PC1 and PC2 exhibit a higher-order trend which could be spurious and is likely to originate from the observing system changes like 1979 start of the satellite observations era) and a linear trend in the transports. The largest transports occur when the second wind stress curl mode has a cyclonic/anticyclonic anomaly in its subtropical/subpolar center of activity. These curl anomalies, in the late 1960s and after 2001, are consistent with a weak subtropical and subpolar gyre. Also the tracer model results in section 3.2 suggest that the strongest northward upper ocean penetration coincides with the weakest subtropical gyre in these two epochs.

4.2. Model Response to Modulation of the Wind Stress Curl Strength

[22] So far we have only dealt with possible connections between basin-scale atmospheric forcing and the northward flux of high-salinity water, but we have not discussed what is the actual dynamic process leading to the enhanced northward advection of high-salinity waters in the northeastern Atlantic. We give a simple schematic (Figure 13) showing how outcropping and subpolar front formation varies with the intensity of wind forcing; this front guides subtropical waters into the subpolar gyre even when the Sverdrup vertical integral of transport has no intergyre circulation. When the wind stress curl mode 2 suggests much stronger amplitude curl

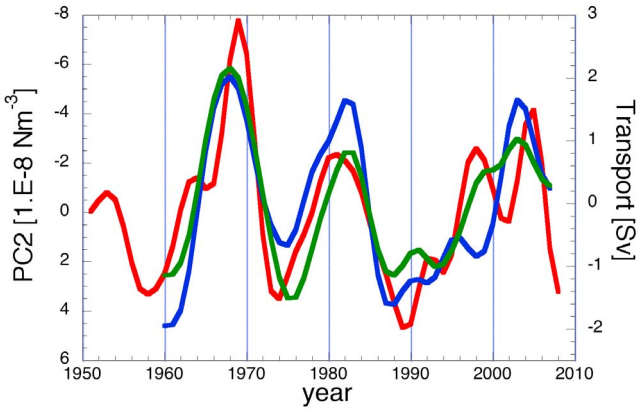

Figure 12. Relationship between wind stress curl PC2 (red) and northward transport anomalies of the highest salinity classes (S > 35.3 psu; blue and S > 35.4 psu; green) at 55°N. All quantities are 5 year running means and detrended.

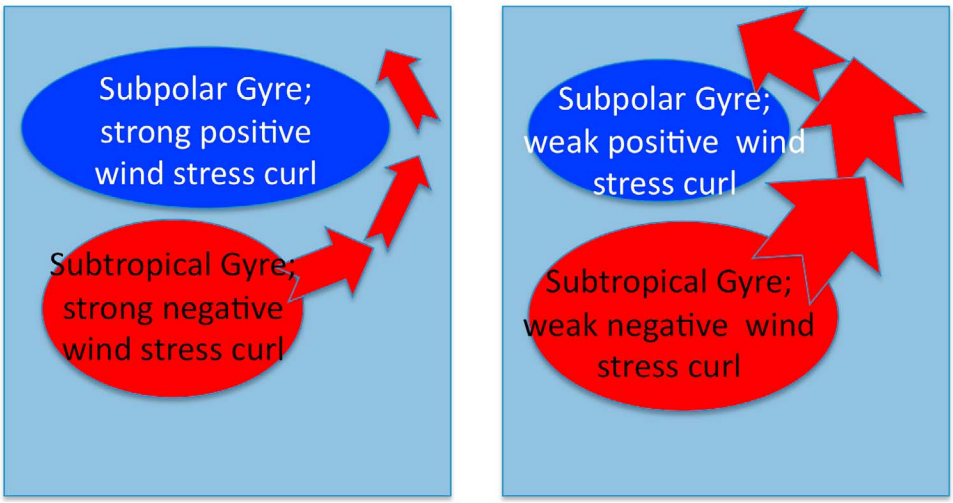

Figure 13. The modulation of the wind stress curl amplitude resembling the EOF mode 2 (and the climatological pattern) and its impact on the gyres.

with the climatological curl pattern, both gyres intensify such that the subpolar gyre expands and the polar front moves eastward, while the subtropical gyre contracts and deepens (Figure 13, left). In the opposite case, the subpolar density surfaces relax and the polar front moves westward and the subtropical gyre relaxes and expands (Figure 13, right). A net result of the weakening of the gyres is that the eastern boundary region widens in the subpolar gyre allowing paths of high-salinity waters from the expanding subtropical gyre to the northern gyre. This wind-driven gyre effect can, in fact, be behind the gyre mode described by *Hátún et al.* [2005, Figure 3], although they did not specifically attribute its dynamics to the wind stress curl variability.

[23] The tracer advection study in section 3.2 suggests that the most prominent northward reach of the saline subtropical surface waters occurred when the subtropical gyre was weak. Also in section 4.1 we show that the second wind stress curl mode projects on the gyres and the low-pass-filtered PC2 of the curl indeed resembles the transport estimates of the most saline flow components at 55°N. We apply an asymmetric, zonally constant, wind stress curl with zero line at 50°N (Figure 14) to force a two-layer model, the Hallberg Isopycnal Model (HIM) [*Hallberg*, 2000, available at https://fms.gfdl.noaa.gov/gf/]. We use upper layer thickness of 500 m and lower-layer thickness of 1500 m with a flat bottom, and a density difference of 1.5 sigma units. Spatial resolution was 0.5°, and model domain was 80°W to 5°W and 20°N to 65°N.

[24] In this simplest possible context we show how the outcropping geometry of the subpolar gyre can force subtropical warm waters northeastward across the zero wind curl line, even in absence of buoyancy forcing and its AMOC. We spun up the HIM model for 50 years and created two additional 5 year simulations with 20% stronger and 20% weaker wind stress curl (Figure 14). The integrated stream function and upper layer thickness in the two anomaly cases at the end of the 5 years is shown in Figure 15. The vertically integrated stream function displays well-defined gyres where the strong wind stress curl simulation shows more intense circulation in the gyre centers as expected. In the upper layer thickness patterns the most prominent feature is the penetration from subtropical to subpolar gyres in the "northeast corner" of the basin. This occurs in spite of the zonally constant but opposing sign Sverdrup transport, in which the two gyres do not communicate geostrophically. As the upward Ekman pumping in the subpolar zone causes the thermocline to outcrop, the subpolar cold surface gyre recedes to the west, and warm water penetrates far northward to compensate. This occurs in absence of any buoyancy forcing or classical MOC.

[25] By decreasing the strength of the wind stress curl, the layer thickness (Figure 15) shows the movement and spreading of the eastern boundary front westward effectively widening the window for the subtropical waters to penetrate

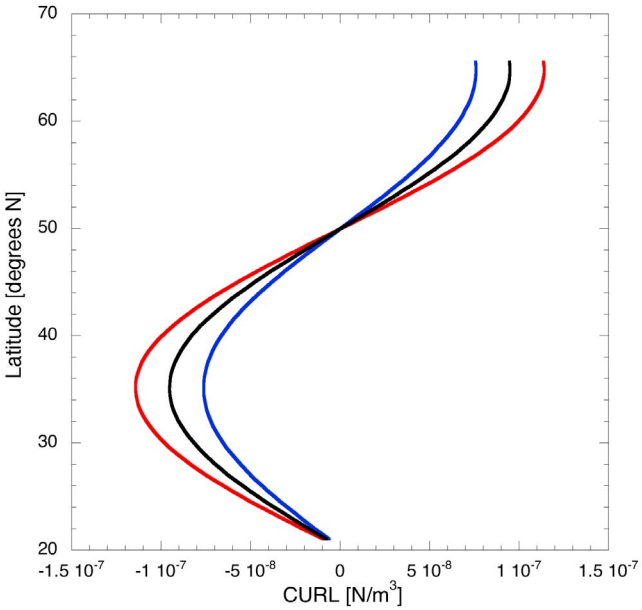

Figure 14. Wind stress curl cross section (constant in longitude) in the control run (black), strong case (red) and weak case (blue).

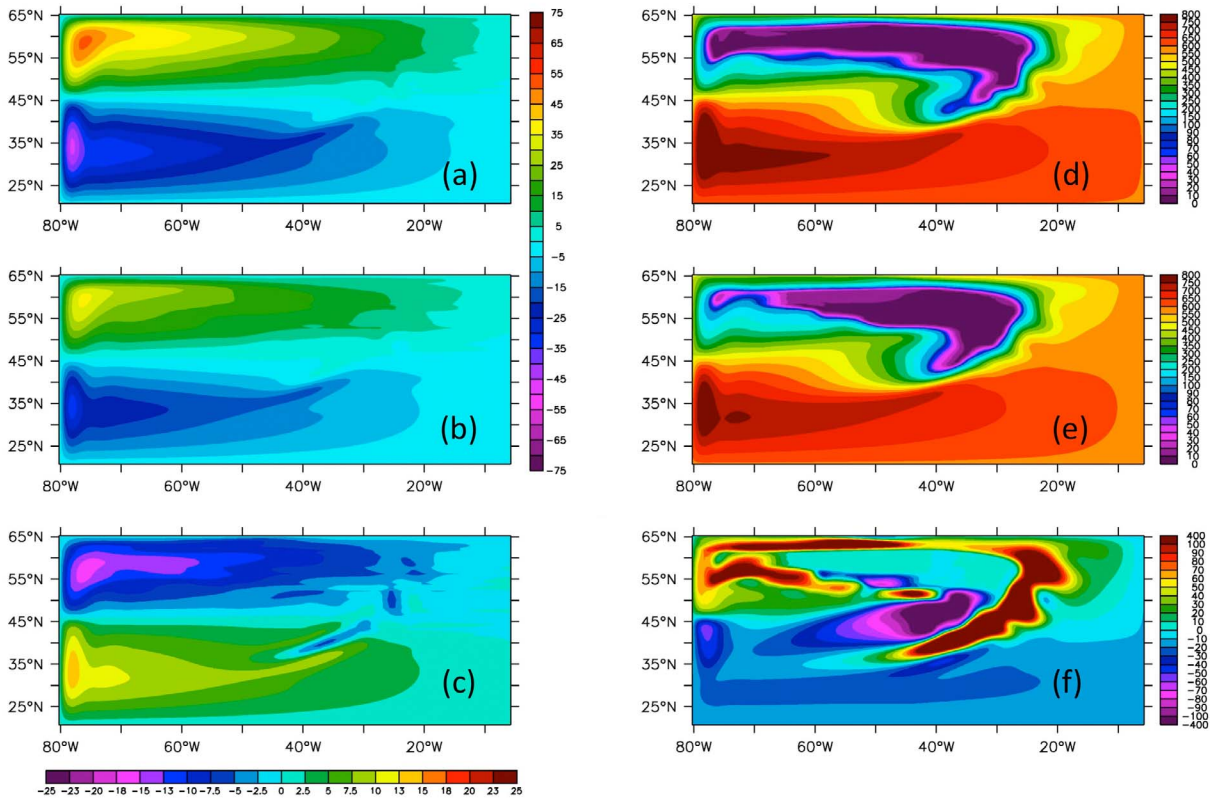

Figure 15. (a–c) Vertically integrated stream function and (d–f) upper layer thickness from the HIM model, averaged over 5 years in the case of 20% stronger (Figures 15a and 15d) or 20% weaker (Figures 15b and 15e) curl than in the control run of 50 years which was used to initialize the 5 year anomalous curl simulations. The difference low-high curl is shown in Figures 15c and 15f. Units are in Sv for stream function and meters for layer thickness.

the subpolar gyre. The effect of the westward movement on tracer pathways is demonstrated with two sets of experiments corresponding to the strong curl and weak curl results from HIM model. We used our tracer advection model discussed earlier with a constant 5 year average velocity field and keeping the tracer value constant in a box defined as 70°W–55°W, 40°N–45°N in the western subtropical gyre. The results from these tracer model experiments are shown in Figures 16 supporting the SODA result: the tracers advect northward into the subpolar region more efficiently in the case of a weak wind stress curl amplitude and associated weak gyres. The westward movement of the upper layer front in case of a weak subpolar gyre allows the tracers escape the subtropical gyre in greater concentrations than in the strong curl case. In case of a strong subtropical gyre (and strong curl), the further east the tracers travel, the higher the probability that they will be caught in the southward currents of the subtropical gyre. The northward access of subtropical waters in the weak wind stress curl case occurs through the change in the source of the northward tracer transport and not through the actual northward upper layer (water) velocities in the eastern basin (which are lower in the weak curl case than in the strong curl case as expected). The tracer advection with SODA velocity fields go one step further: the weak gyres retain significant part of the tracers in the gyre in the weak curl case. This effect is not apparent in this simple model with closed boundaries and an idealistic two-layer structure.

[26] These tracer experiments with the two-layer HIM model velocity fields are somewhat sensitive where one sets the tracer box. A wide variety of box locations north of the subtropical gyre center (~32°N) gives results similar to the example here. However, moving the box northward to 42°N–47°N reverses this behavior; this box straddles both the subtropical and subpolar gyres and the tracer spreading is determined by the subpolar gyre circulation which follows the strength of the wind stress curl.

5. Conclusions

[27] The high-salinity conditions in the NE Atlantic since late 1990s, but more pronounced after 2000, are highly unusual with the most recent prior occurrence in the late 1960s. The early 2000s conditions were associated with a large-scale shift in surface currents recorded by the surface drifter data [*Hakkinen and Rhines*, 2009]. The historical data viewed through the SODA assimilation provide an opportunity to investigate the atmospheric and oceanic conditions during these high-salinity events. The SODA data also provide a view of the changes in meridional overturning circulation, but we focus primarily on the changes of the vertical structure in the upper limb of AMOC. The variable penetration of subtropical waters poleward may involve many local and distant forcing effects. We have singled out wind stress curl variability as a proximate cause. The other forcing effects local to the subpolar

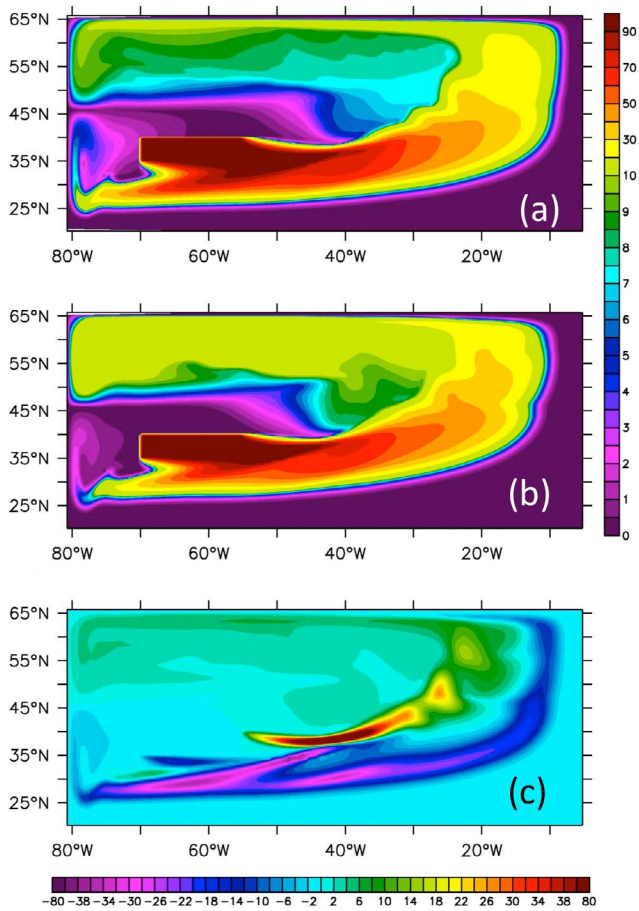

Figure 16. Tracers release into the HIM model upper layer circulation in a box 70°W–55°W, 35°N–40°N in the case of (a) a strong curl, (b) a weak curl, and (c) the difference weak-strong curl. Concentration (unitless) is shown at the end of 5 year simulation.

North Atlantic include air/sea buoyancy flux, Greenland tip jet events, and recurring blocking patterns.

[28] The shifts in the surface circulation can be elucidated through tracer advection in an offline advection model. Tracer advection is a good analogy for the salinity advection because the upper ocean density variability is determined almost completely by temperature in the subtropical waters. Our tracer experiments for depth of 15 m show that both the 1960s and early 2000s are the only time periods with apparent penetration of subtropical waters originating from the Gulf Stream region to the NE Atlantic. Usually the preceding periods, the early 1960s, late 1970s and late 1990s, also have somewhat stronger northward extent of subtropical waters.

[29] Hydrographic data as reconstructed by the SODA assimilation system shows that the high-salinity events were peaking near surface but reaching as deep as 1000 m and hence pointing to large-scale gyre circulation changes. Atmospheric forcing can locally drive variability in the subpolar mode water production [e.g., *Johnson and Gruber*, 2007] which coexists with effects of variable subtropical/subpolar gyre exchange. To address the atmospheric forcing of the circulation changes, we computed EOF analysis for the wind stress curl which results in the monopole and dipole patterns. The monopole pattern (26%) has a center of activity west of the British Isles, which fluctuates closely with the NAO index. The second (dipole) mode (17%) has centers similar to NAO loading pattern but its PC has weaker correlation with NAO index. This second curl mode projects onto the strength of the subtropical and subpolar gyres because it has a similar structure as the climatological wind stress curl. SODA data shows that the transport of the highest salinity components varies with the phase of the PC of the second mode such that the transport maxima occur when the wind stress curl anomaly is cyclonic (anticyclonic) in the subtropics (subpolar gyre). The phasing of the curl anomalies opposite to the climatological curl pattern is consistent with weakened gyres in both subtropical and subpolar regions.

[30] It is not obvious why the subtropical waters should have an easier access to the higher latitudes when the gyres are weak. We know from the model experiment of *Hátún et al.* [2005] and observations by *Bersch* [2002] and *Bersch et al.* [2007] that in the late 1990s with the weak/negative NAO index, the polar front moved westward to allow the saline water components to move northward. We use a more general case of an idealized two-layer isopycnal model [*Hallberg* 2000] to show that by modulating the strength of the dipole wind stress curl pattern, which resembles the average wind stress curl, subtropical tracers were able to spread northward to the subpolar gyre more efficiently with a weaker than normal wind stress curl forcing. This cross-gyre penetration relates to the presence of density-surface outcropping in the subpolar gyre, and hence to the east-west location of the subpolar front. The weakness of both gyres allowed the eastern boundary front to move westward opening a wide window for the subtropical waters to move northward. This wind stress driven response impacts the composition of the AMOC upper limb water masses at the northern latitudes even without the presence of buoyancy forcing variations.

[31] The failure of the NAO index to predict the saline event after 2001 (as compared with the 1960s and late 1970s events) showed that sea level pressure index is not always adequate to describe the ocean response to the atmospheric variability. We find that the standard EOF analysis of the wind stress curl does not give the most important mode as the leading mode when considering the gyre strength. We show that the second EOF mode of the wind stress curl has a larger impact than the first mode, because it readily projects on the Atlantic Ocean gyres by modulating the wind stress curl pattern which formed the gyres in the first place. The temporal variability of the second wind stress curl mode contains many features of the NAO variability but appears to represent a separate entity imbedded to the NAO and storm track variability.

[32] **Acknowledgments.** We sincerely thank both of our referees for constructive criticism and helpful comments to improve the manuscript. S.H. and D.L.W. gratefully acknowledge the support from NASA Headquarters Physical Oceanography Program and OSTM Science Team for this work. P.B.R. is supported by NASA through the OSTM Science Team.

References

Belkin, I. M., S. Levitus, J. Antonov, and S.-A. Malmberg (1998), Great salinity anomalies in the North Atlantic, *Prog. Oceanogr.*, *41*, 1–68, doi:10.1016/S0079-6611(98)00015-9.

Bersch, M. (2002), North Atlantic Oscillation–induced changes of the upper layer circulation in the northern North Atlantic Ocean, *J. Geophys. Res.*, *107*(C10), 3156, doi:10.1029/2001JC000901.

Bersch, M., I. Yashayev, and K. M. Koltermann (2007), Recent changes of the thermohaline circulation in the subpolar North Atlantic, *Ocean Dyn.*, *57*, 223–235, doi:10.1007/s10236-007-0104-7.

Brambilla, E., and L. D. Talley (2006), Surface drifter exchange between the North Atlantic subtropical and subpolar gyres, *J. Geophys. Res.*, *111*, C07026, doi:10.1029/2005JC003146.

Brambilla, E., and L. D. Talley (2008), Subpolar mode water in the northeastern Atlantic: 1. Averaged properties and mean circulation, *J. Geophys. Res.*, *113*, C04025, doi:10.1029/2006JC004062.

Brambilla, E., L. D. Talley, and P. E. Robbins (2008), Subpolar mode water in the northeastern Atlantic: 2. Origin and transformation, *J. Geophys. Res.*, *113*, C04026, doi:10.1029/2006JC004063.

Carton, J. A., and B. S. Giese (2008), A reanalysis of ocean climate using Simple Ocean Assimilation System (SODA), *Mon. Weather Rev.*, *136*, 2999–3017, doi:10.1175/2007MWR1978.1.

Carton, J. A., G. Chepurin, X. Cao, and B. Giese (2000), A simple ocean data assimilation analysis of the global upper ocean 1950–95. Part I: Methodology, *J. Phys. Oceanogr.*, *30*, 294–309, doi:10.1175/1520-0485(2000)030<0294:ASODAA>2.0.CO;2.

Dickson, R. R., R. R. Dickson, J. Meincke, S.-A. Malmberg, and A. J. Lee (1988), The 'Great Salinity Anomaly' in the northern North Atlantic 1968–1982, *Prog. Oceanogr.*, *20*, 103–151, doi:10.1016/0079-6611(88)90049-3.

Enfield, D. B., A. M. Mestas-Nunez, and P. J. Trimble (2001), The Atlantic multidecdal oscillation and its relation to rainfall and river flows in the continental US, *Geophys. Res. Lett.*, *28*, 2077–2080, doi:10.1029/2000GL012745.

Hakkinen, S., and P. B. Rhines (2009), Shifting surface currents in the northern North Atlantic Ocean, *J. Geophys. Res.*, *114*, C04005, doi:10.1029/2008JC004883.

Hallberg, R. (2000), Time integration of diapycnal diffusion and Richardson number-dependent mixing in isopycnal coordinate ocean models, *Mon. Weather Rev.*, *128*(5), 1402–1419, doi:10.1175/1520-0493(2000)128<1402:TIODDA>2.0.CO;2.

Hansen, B., S. Østerhus, W. R. Turrell, S. Jonsson, H. Valdimarsson, H. Hatun, and S. M. Olsen (2008), The inflow of Atlantic water, heat and salt to the Nordic Seas across the Greenland-Scotland Ridge, in *Arctic-Subarctic Ocean Fluxes: Defining the Role of the Northern Seas in Climate*, edited by R. R. Dickson, J. Meincke, and P. B. Rhines, pp. 15–43, Springer, Dordrecht, Netherlands.

Harnik, N., and E. C. Chang (2003), Storm track variations as seen in radiosonde observations and reanalysis data, *J. Clim.*, *16*, 480–495, doi:10.1175/1520-0442(2003)016<0480:STVASI>2.0.CO;2.

Hátún, H., B. Hansen, A. B. Sandø, H. Drange, and H. Valdimarsson (2005), De-stabilization of the North Atlantic thermohaline circulation by a gyre mode, *Science*, *309*, 1841–1844, doi:10.1126/science.1114777.

Holliday, N. P. (2003), Air-sea interaction and circulation changes in the northeast Atlantic, *J. Geophys. Res.*, *108*(C8), 3259, doi:10.1029/2002JC001344.

Holliday, N. P., et al. (2008), Reversal of the 1960s–1990s freshening trend in the north-east North Atlantic and Nordic Seas, *Geophys. Res. Lett.*, *35*, L03614, doi:10.1029/2007GL032675.

Johnson, G. C., and N. Gruber (2007), Decadal water mass variations along 20°W in the northeastern Atlantic Ocean, *Prog. Oceanogr.*, *73*, 277–295, doi:10.1016/j.pocean.2006.03.022.

Kalnay, E., et al. (1996), The NCEP/NCAR 40-year reanalysis product, *Bull. Am. Meteorol. Soc.*, *77*, 437–471, doi:10.1175/1520-0477(1996)077<0437:TNYRP>2.0.CO;2.

Lin, S.-J., W. C. Chao, Y. C. Sud, and G. K. Walker (1994), A class of van Leer-type transport schemes and its application to the moisture transport in a general circulation model, *Mon. Weather Rev.*, *122*, 1575–1593, doi:10.1175/1520-0493(1994)122<1575:ACOTVL>2.0.CO;2.

Lozier, M. S., and N. M. Stewart (2008), On the temporally varying northward penetration of Mediterranean Overflow Water and eastward penetration of Labrador Sea Water, *J. Phys. Oceanogr.*, *38*, 2097–2103, doi:10.1175/2008JPO3908.1.

McCartney, M. S., and C. Mauritzen (2001), On the origin of the warm inflow to the Nordic seas, *Prog. Oceanogr.*, *51*, 125–214, doi:10.1016/S0079-6611(01)00084-2.

Pollard, R. T., J. F. Read, and N. P. Holliday (2004), Water masses and circulation pathways through the Iceland Basin during Vivaldi 1996, *J. Geophys. Res.*, *109*, C04004, doi:10.1029/2003JC002067.

Reverdin, G. (2010), North Atlantic subpolar gyre surface variability (1895–2009), *J. Clim.*, *23*, 4571–4584, doi:10.1175/2010JCLI3493.1.

Reverdin, G., D. Cayan, and Y. Kushnir (1997), Decadal variability of hydrography in the upper northern North Atlantic in 1948–1990, *J. Geophys. Res.*, *102*, 8505–8531, doi:10.1029/96JC03943.

Rossby, T., C. N. Flagg, and K. Donohue (2005), Interannual variations in upper-ocean transport by the Gulf Stream and adjacent waters between New Jersey and Bermuda, *J. Mar. Res.*, *63*, 203–226, doi:10.1357/0022240053693851.

Sarafanov, A., A. Falina, A. Sokov, and A. Demidov (2008), Intense warming and salinification of intermediate waters of southern origin in the eastern subpolar North Atlantic in the 1990s to mid-2000s, *J. Geophys. Res.*, *113*, C12022, doi:10.1029/2008JC004975.

Yashayaev, I., H. van Aken, N. P. Holliday, and M. Bersch (2007), Transformation of the Labrador Sea Water in the subpolar North Atlantic, *Geophys. Res. Lett.*, *34*, L22605, doi:10.1029/2007GL031812.

S. Häkkinen and D. L. Worthen, NASA Goddard Space Flight Center, Code 614.1, Greenbelt, MD 20771, USA. (sirpa.m.hakkinen@nasa.gov)

P. B. Rhines, School of Oceanography, University of Washington, Box 357940, Seattle, WA 98195, USA.